Catalytic coupling of the active sites in Acetyl-CoA synthase, a bifunctional CO-channeling enzyme

ARTICLE *in* BIOCHEMISTRY · DECEMBER 2001

Impact Factor: 3.02 · DOI: 10.1021/bi015604 · Source: PubMed

2 AUTHORS, INCLUDING:

Ernest L. Maynard
Novavax
22 PUBLICATIONS **405** CITATIONS

SEE PROFILE

Catalytic Coupling of the Active Sites in Acetyl-CoA Synthase, a Bifunctional CO-Channeling Enzyme†

Ernest L. Maynard‡ and Paul A. Lindahl*,§

Department of Chemistry and Department of Biochemistry and Biophysics, Texas A&M University, College Station, Texas 77843-3255

Received July 25, 2001; Revised Manuscript Received August 30, 2001

ABSTRACT: Acetogenic bacteria contain acetyl-CoA synthase (ACS), an enzyme with two distinct nickel−iron−sulfur active sites connected by a tunnel through which CO migrates. One site reduces CO_2 to CO, while the other synthesizes acetyl-CoA from CO, CoA, and the methyl group of another protein (CH_3−CP). Rapid binding of CO_2 and a two-electron reduction activates ACS. When CoA and CH_3−CP bind ACS, CO is rerouted through the tunnel to the synthase site, and kinetic parameters at the reductase site are altered. Under these conditions, the rates of CO_2 reduction and acetyl-CoA synthesis are synchronized by an ordered catalytic mechanism.

Multifunctional enzymes catalyze different types of reactions at spatially distinct active sites. If a product generated at one site is a substrate for the other, a solvent-inaccessible tunnel in the protein is often found to connect the two sites and serve as a one-dimensional pathway for transporting or channeling the intermediate. Intra- and interenzyme channeling of metabolites in cells may be more common than is currently realized (*1*).

The best-studied tunnel-containing enzymes belong to the amidotransferase family and are involved in amino acid (*1*−*3*) and de novo purine (*4*) biosynthesis. Ammonia, indole, carboxy phosphate, and carbamoyl phosphate migrate through solvent-inaccessible tunnels in these enzymes. Multifunctional enzyme mechanisms include not only reactions occurring at each active site but also the means by which the sites interact. Many mechanistic aspects of these complex enzymes have been elucidated. However, because of difficulties in selectively inactivating particular sites and in monitoring intermediates in real-time, important details of active site interactions remain unexplored. In this study, the catalytic mechanism of a relatively simple tunnel-containing enzyme for which such difficulties are overcome is examined.

Acetyl-CoA synthase (ACS[1]) is found in evolutionarily primitive archaea and bacteria, many of which are anaerobic thermophiles that grow chemolithoautotrophically on simple inorganic molecules (CO_2, H_2, N_2 etc.) (*5*−*7*). ACS from *Clostridium thermoaceticum* is an $\alpha_2\beta_2$ tetramer that catalyzes two reactions (1 and 2), one of which is the reversible reduction of CO_2 to CO using low-potential reductants such as reduced methyl viologen (MV^{1+}) (*8*):

$$CO_2 + 2H^+ + 2MV^{1+} \rightleftarrows CO + H_2O + 2MV^{2+} \quad (1)$$

$$CO + CH_3{-}CP^{n+} + CoASH \rightleftarrows CH_3C(O)SCoA + CP^{(n-1)+} + H^+ \quad (2)$$

The C-cluster active site for this reductase activity is a Ni−Fe−S-containing cluster located in the β subunit (9). The X-ray diffraction crystal structure of an enzyme (from *Carboxydothermus hydrogenoformans*) homologous to the β_2 dimeric unit of ACS has just been reported (*10*).

The other reaction catalyzed is the synthesis of acetyl-CoA from CO (or CO_2 and $2MV^{1+}$), Coenzyme A, and a methylated corrinoid-iron−sulfur protein (CH_3−CP). The methyl group of CH_3−CP is transferred from CH_3−THF in a reaction catalyzed by a methyltransferase (MT). The A-cluster active site for this synthase activity is a different Ni−Fe−S cluster located in the α subunit (*9*). The two clusters are magnetically isolated and undoubtedly separated by >10 Å (*10*, *11*). A symbolic representation of ACS is given in Figure 1. CO can be trapped with hemoglobin (Hb), a rapid and tight binding "CO sensor" (*12*). During the ACS-catalyzed synthesis of acetyl-CoA using CO_2 and MV^{1+} rather than CO as substrates, the presence of Hb does not inhibit catalysis, indicating a solvent-inaccessible molecular tunnel through which CO migrates from the C- to the A-cluster (*13*).

EXPERIMENTAL PROCEDURES

ACS, CP, and MT, purified from *C. thermoaceticum* (ATCC 39073) cell paste (*14*, *15*), have molecular weights of 154 700 (*16*), 89 000 (*17*), and 57 280 (*18*), respectively. Buffers had CO_2 concentrations of ∼5 μM (*14*). MV^{1+} was prepared enzymatically (*14*). Concentrations of stock CH_3−

* To whom correspondence should be addressed. Phone: 979-845-0956. FAX: 979-845-4719. E-mail: Lindahl@mail.chem.tamu.edu.

† The National Institutes of Health (GM46441) and the Robert A. Welch Foundation (A1170) sponsored this study.

‡ Department of Chemistry.

§ Department of Biochemistry and Biophysics.

[1] Abbreviations: ACS, acetyl-CoA synthase, also known as CODH, carbon monoxide dehydrogenase; phen−ACS, ACS treated with 1,10-phenanthroline and lacking labile Ni in functional A-clusters; CN-ACS, ACS treated with cyanide ion and with CN^- bound to the C-cluster; CoA, coenzyme A; THF, tetrahydrofolate; MV, methyl viologen; CP, corrinoid iron sulfur protein; MT, methyl transferase.

10.1021/bi015604+ CCC: $20.00
Published on Web 10/13/2001

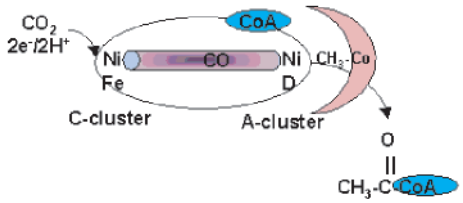

FIGURE 1: Symbolic representation of ACS. The large ellipse represents ACS, with the C-cluster on the left, the A-cluster on the right, and the tunnel in the center. The crescent and small ellipse indicate CP and CoA, respectively. "Ni Fe" and "Ni D" designate the C- and A-clusters ("D" represents the D-site) of ACS, while "Co" represents the cobalamin in CP.

THF (*19*, *20*) and CoA (*21*) solutions were calculated using their extinction coefficients. The Henry's Law constant for CO_2 at 30 °C is 31 mM·atm^{-1} (*22*).

Different combinations of 50 mM MES pH 6.3 buffer, CH_3−THF (2.0 mM), CP, MT, MV^{1+} (1.0 mM), Hb (17 μM $\alpha_2\beta_2$), CO, and CO_2 were prepared in a reaction vessel (*13*) and transferred via a needle-to-Luer-tip adaptor to one syringe of a stopped-flow (SF) system (Hi-Tech SF-61 DX2 Double Mixing System) located inside of a glovebox (MJ Braun) maintained at ~1 ppm O_2. To the other SF syringe was added different combinations of buffer, CoA (1.0 mM), DTT (50 μM), and ACS. The concentrations mentioned here and in the text are final values after mixing equal volumes from each SF syringe. Prior to reaction, solutions inside of the water-jacketed SF syringes were incubated for 10 min at 30.0 ± 0.1 °C in dim light. SF data from 2 to 3 shots were averaged.

RESULTS AND DISCUSSION

The apparent k_{cat} and K_m for CO_2 in the ACS-catalyzed synthesis of acetyl-CoA are 200 ± 30 min^{-1} and 380 ± 40 μM, respectively, as determined previously by monitoring the production of acetyl-CoA at pH 6.3 and in the presence of MV^{1+} and the "synthase substrates" (CoA and CH_3−CP) (*14*). An equivalent experiment was performed in the absence of the synthase substrates, causing ACS to catalyze only the reduction of CO_2 to CO. In this "reductase mode", the apparent k_{cat} and K_m for CO_2 were 37 ± 4 min^{-1} and 7000 ± 1000 μM, respectively, as determined by monitoring either MV^{1+} utilization or CO production (data not shown). These kinetic parameters are substantially different from those obtained when ACS operates in "synthase mode"; e.g., k_{cat}/K_m differs by ~100 fold.

Similar kinetic values were obtained when Hb was included under reductase conditions, discounting the possibilities that the rates differed because CO accumulated with ACS in reductase mode and that this built up inhibited catalysis. Rather, the shift in the CO_2 kinetic parameters at the C-cluster was probably triggered either by the binding of one or both synthase substrates at or near the A-cluster or by a step in the synthase mechanism occurring after that binding. The triggering event then propagated from the vicinity of the A-cluster to the C-cluster via a protein conformational change. The triggering, propagation, and shift in parameters will collectively be called *A → C coupling*.

To determine whether the trigger for A → C coupling was the binding of one or both synthase substrates, rates of CO production and MV^{1+} utilization were measured simultaneously in steady-state assays containing Hb and various combinations of synthase substrates (Figure 2). A → C coupling, as indicated by the increased rate of MV^{1+} utilization, occurred only when both synthase substrates were included (Figure 2C), suggesting that the trigger is either the simultaneous binding of the synthase substrates or a mechanistic step in the synthesis of acetyl-CoA.

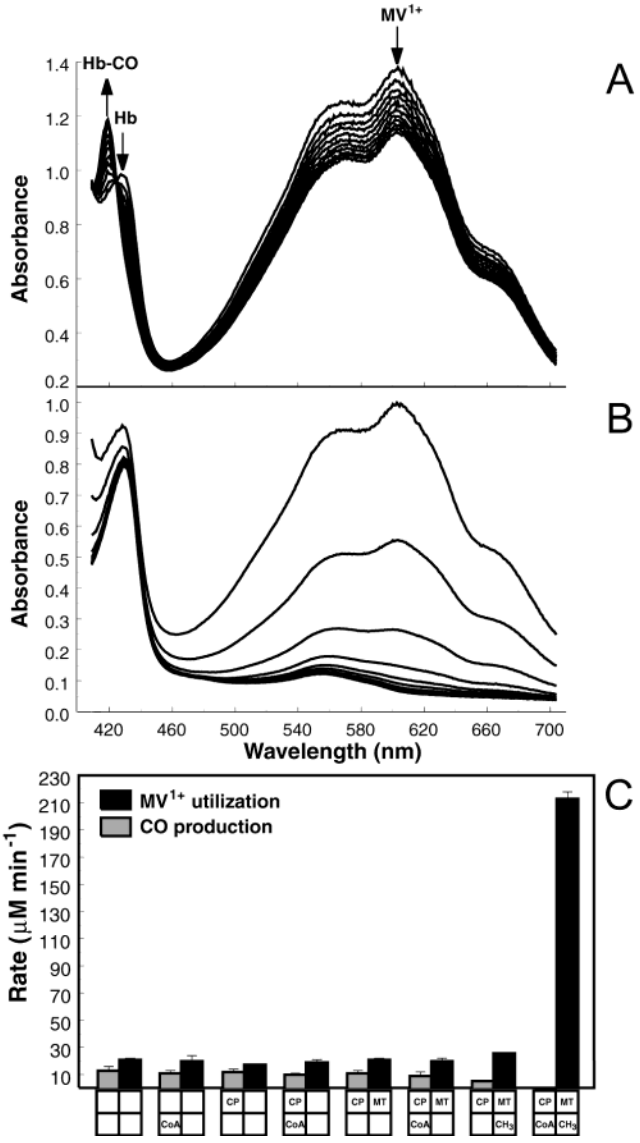

FIGURE 2: Photodiode-array time-resolved spectra of stopped-flow solutions of ACS in reductase (A) and synthase (B) modes and a bar-graph comparison of MV^{1+} utilization and CO production under different conditions (C). In panel A, a CO_2-saturated solution containing MV^{1+} and Hb was reacted with ACS (0.3 μM $\alpha\beta$). Selected spectra were acquired at 73.5 s intervals, with the first at 0.75 s. Conditions in panel B were identical, except that CH_3−THF, CP (30 μM $\alpha\beta$), and MT (10 μM α_2) were added to the CO_2/MV/Hb syringe and CoA was added to the ACS syringe. In panel C, rates of CO production and MV^{1+} utilization were determined in the presence of different combinations of ACS, CoA, CH_3−THF ("CH_3"), CP, and MT, as indicated by the boxes under the bar-graphs.

Also correlated with coupling was the cessation of CO production, as evidenced by the absence of Hb−CO formation when the enzyme operated in synthase mode (Figure 2B,C). Thus, A → C coupling reroutes CO. Uncoupled ACS reduces CO_2 and releases CO into solution. Coupled ACS

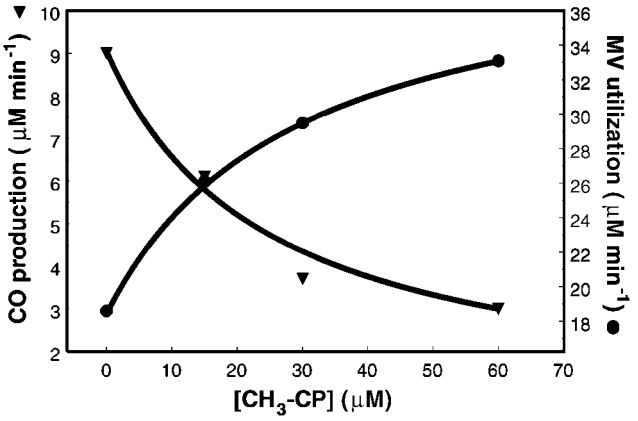

FIGURE 3: Analysis of CP binding to phen-treated ACS. Phen-treated ACS (*23*) was used in SF reactions. Conditions were as described in Figure 2B, except that CH_3-CP was varied from 0 to 60 μM $\alpha\beta$. As expected, the phen−ACS sample had no synthase activity but had CO oxidation activity typical of native enzyme.[5]

transports the C-cluster-synthesized CO through the tunnel to the A-cluster for use in acetyl-CoA synthesis. The results in Figure 2 also reveal that there is no "leakage" of CO from the enzyme in synthase mode. Thus, A → C coupling synchronizes the rates of the two catalytic reactions occurring at different clusters and locations in the enzyme.

The rate of reductase catalysis was also determined by monitoring Hb−CO formation (Figure 2C). As expected, the rate was similar to that obtained by monitoring the utilization of MV^{1+}. In contrast, the apparent k_{cat} for acetyl-CoA synthesis (i.e., under synthase conditions) calculated from MV^{1+} utilization (350 min^{-1}) was substantially faster than that obtained by measuring the formation of acetyl-CoA (200 min^{-1}). This suggests that A → C coupling activates an unidentified redox reaction (with an apparent $k_{cat} \sim 150$ min^{-1}) in which MV^{1+} is the reductant but neither CO nor acetyl-CoA (nor H_2)[2] are products.

Treating ACS with 1,10-phenanothroline (phen) removes the Ni ion of the A-cluster and selectively inactivates the synthase activity (*23*). This process appears to have little affect on the gross structure of the enzyme, as the reductase activity, the spectroscopic features of the other clusters in the enzyme, and the ability to bind CoA are unaffected. Moreover, incubating phen−ACS in $NiCl_2$ reinserts Ni into the apo-A-cluster, restoring synthase activity and spectroscopic features of the native A-cluster.

When phen−ACS was used in the synthase assay lacking CH_3-CP, rates of CO production and MV^{1+} consumption were essentially the same as those obtained with native ACS operating in reductase mode. However, at increasing $[CH_3-CP]$, the rate of CO production declined while the MV^{1+} consumption rate increased (Figure 3). An apparent K_d of 24 μM for the binding of CH_3-CP to phen−ACS was calculated from the plot of [CO] production versus $[CH_3-CP]$. More importantly, at infinite $[CH_3-CP]$, the calculated rates of CO production and MV^{1+} utilization were ~ 6% and ~200%, respectively, of the equivalent values for native ACS in reductase mode. The absence of CO production characterizes native ACS operating in synthase mode,

[2] Using a reaction vessel containing 0.5 mL of headspace, 7 mM MV^{1+}, 4 mM CH_3-THF, 4 mM CoA, 10 μM MT, and 10 μM ACS, no H_2 was detected by GC in the headspace after 30 min reaction.

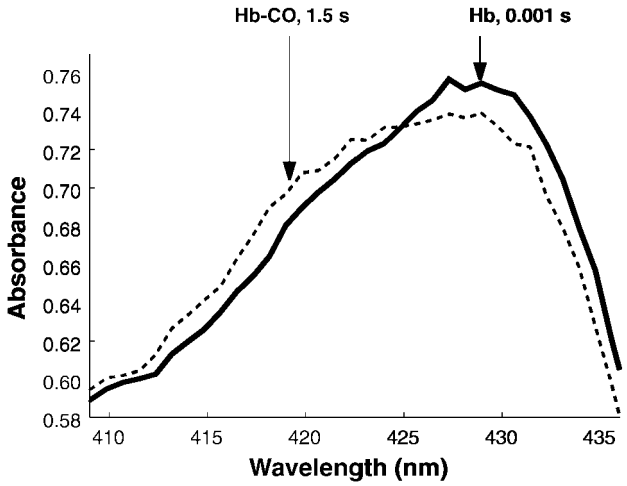

FIGURE 4: Pre-steady-state formation of CO as ACS converts from reductase to synthase mode. Solutions were identical to those described in Figure 2B, except that ACS and MT concentrations were 20 μM $\alpha\beta$ and 170 μM α_2, respectively. Hb Soret bands were monitored.

and it suggests that under these conditions, phen−ACS is unable to reduce CO_2 to CO. On the other hand, the increased utilization of MV^{1+} was unexpected, as phen−ACS is unable to synthesize acetyl-CoA. The maximum rate of MV^{1+} utilization corresponds to $k_{cat} \sim 130$ min^{-1} and is probably due to the unidentified redox reaction alluded to above. This experiment reveals that ACS need not actively catalyze the synthesis of acetyl-CoA to be A → C coupled and in the synthase mode; coupling simply requires that both synthase substrates bind to ACS. However, the Ni also appears to be involved, since under identical conditions with native ACS, no CO would have been made. This experiment also suggests that the unidentified MV^{1+}-utilizing redox reaction is activated when the enzyme is A → C coupled and that this reaction is not involved in CO or acetyl-CoA formation.

Small amounts of CO (~6 μM) were formed in pre-steady-state assays when native ACS and synthase substrates were mixed (Figure 4), and this allowed the rate at which ACS converts from reductase to synthase mode to be estimated. Assuming that $[ACS_r] \rightarrow [ACS_s]$ is a first-order process defined by rate-constant $k_{r\rightarrow s}$, the time-dependence of CO formation is given by eq 3:

$$[CO]_t = \frac{k_{cat-r}}{k_{r\rightarrow s}}[ACS_r]_{t=0} - \frac{k_{cat-r}}{k_{r\rightarrow s}}[ACS_r]_{t=0}e^{-k_{r\rightarrow s}t} \quad (3)$$

k_{cat-r} is the apparent k_{cat} for CO_2 reduction under the conditions employed (15.5 mM CO_2), calculated to be 25 min^{-1}. At infinite time, $k_{r\rightarrow s} = k_{cat-r}[ACS_r]_{t=0}/[CO]_{t=\infty}$, suggesting that $k_{r\rightarrow s} \sim 80$ min^{-1} (25 $min^{-1} \times 20$ μM/6 μM).

CO was produced at a linear, steady-state rate in accordance with an apparent first-order rate constant of 40 min^{-1} (Figure 5, panel IA), and as expected, MV^{1+} was oxidized at essentially double that rate ($k_{app} = 70$ min^{-1}; Figure 5, panel I, C). In the first ~ 100 ms of the reaction (prior to achieving steady state), no CO was detected. However, during this pre-steady state period, approximately 2 equiv/$\alpha\beta$ of MV^{1+} were utilized in accordance with a maximum first-order rate-constant $k_{burst} = 1100$ min^{-1} (Figure 5, Panel I, B−D). The magnitude of this "burst" in MV^{1+} utilization was linearly proportional to the ACS concentra-

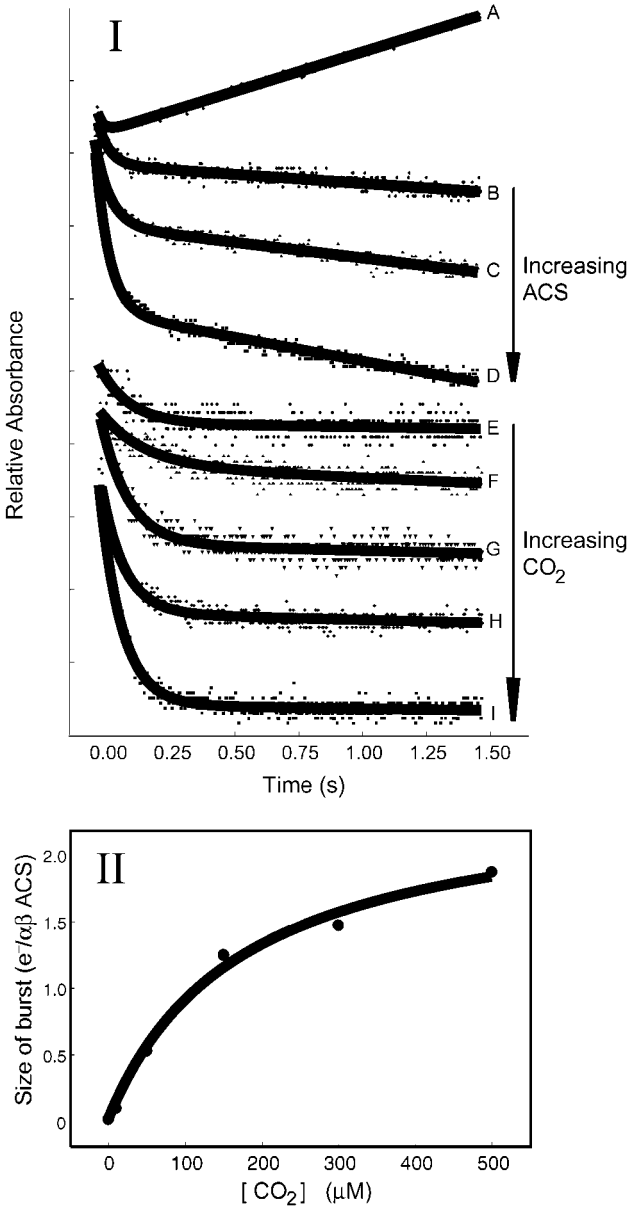

FIGURE 5: Pre-steady-state analysis of CO production and MV^{1+} utilization in the reductase mode (Panel I) and CO_2 dependence of the kinetic burst intensity (Panel II). Solutions were identical to those described in Figure 2A except that [ACS] or [CO_2] was varied. Panel I: (A) Formation of Hb−CO (monitored at 419 nm) using 20 μM $\alpha\beta$ ACS. (B−D). MV^{1+} utilization at [CO_2] = 16 mM and ACS concentrations of 10 (B), 20 (C), or 35 (D) μM $\alpha\beta$. (E−I). MV^{1+} utilization at [ACS] = 20 μM $\alpha\beta$ and CO_2 concentrations of 10 (E), 50 (F), 150 (G), 300 (H), or 500 (I) μM. Other conditions were as in Figure 2A except that Hb was absent. Solid lines are simulations generated by fitting the equation $A_{665} = \beta \exp(-kt) + mt + c$ to the data. In this equation, β is the burst magnitude, k is an apparent first-order decay constant (equal to ~1100 min^{-1} for B−D and 400−700 min^{-1} for E−I), $|m|$ is the steady-state slope, and c is the offset. Panel II: Normalized burst magnitude (β_n) plotted vs [CO_2]. Solid line was generated from the equation $\beta_n = \beta_{n-max}[CO_2]/\{[CO_2] + K_d\}$.

tion, and it fit to a slope of 1.5 equiv/$\alpha\beta$ ACS. The normalized burst magnitude also increased with increasing [CO_2] (Figure 5, Panel I, E−I), and a plot of these data was fitted by a simple binding isotherm with $K_d = 170 \pm 40$ μM and a maximal burst of 2.5 ± 0.4 electrons/$\alpha\beta$ (Figure 5, Panel II). Since this K_d for CO_2 binding in the burst reactions was so much smaller than the K_m for CO_2 in the

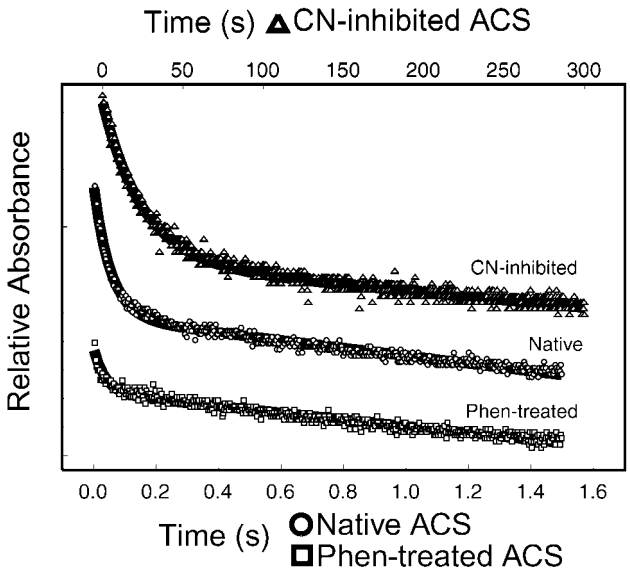

FIGURE 6: Comparison of pre-steady-state MV^{1+} utilization by ACS, phen−ACS, and CN−ACS. CN−ACS (17) had 3% CO oxidation activity relative to native ACS. Other conditions were the same as those described in the Figure 2A except that Hb was absent and [ACS] = 20 μM $\alpha\beta$. The reaction was monitored at 665 nm. The steady-state rate of MV^{1+} utilization after the burst corresponded to ~1% of that observed using native ACS, indicating that CN−ACS was essentially fully inhibited during and after the burst.

reductase mode (7000 μM), this reaction almost certainly does not correspond to substrate binding in the reductase catalytic mechanism. The apparent first-order rate constant associated with the burst did not change significantly with changes in either [ACS] or [CO_2]. Thus, the burst reflects a very rapid, multielectron $n = 2$ (or $n = 4$)[3], CO_2-dependent reduction of ACS. The CO_2 dependence indicates that CO_2 binding precedes and facilitates reduction. The burst reactions yield either a CO-bound form of ACS, or a CO_2-bound form in which another site (possibly the D-site, ref 24) has been reduced.

A burst reaction with the same magnitude could also be detected when ACS was in synthase mode, but the rate was influenced by the MT concentration, and the apparent first-order rate constant varied considerably (k_{burst} = 200−1000 min^{-1}). The burst was faster than the rate-determining step of the reductase mechanism, and given the time required for the system to convert from reductase to synthase mode, it should also precede the synthase reactions.

Cyanide ion binds tightly to an Fe of the C-cluster, blocking reduction of this cluster and inhibiting reductase activity (*25*). Nevertheless, CN-inhibited ACS (CN−ACS) exhibited an initial burst in MV^{1+} consumption (Figure 6), with a magnitude equivalent to that obtained using native ACS (albeit at a 400-fold slower rate; $k_{app} = 2.5$ min^{-1}). This experiment reveals that the site reduced during the burst is not the C-cluster and that the C-cluster need not be redox active for the burst reactions to occur. However, the C-cluster appears to be involved in the kinetics of these processes. Phen−ACS also exhibited a burst in MV^{1+} utilization, with a magnitude ~ 40% that of native enzyme

[3] Due to the heterogeneity of ACS, only ~50% of the enzyme is functional (*22*, *23*). Correcting for this increases the number of electrons by a factor of 2.

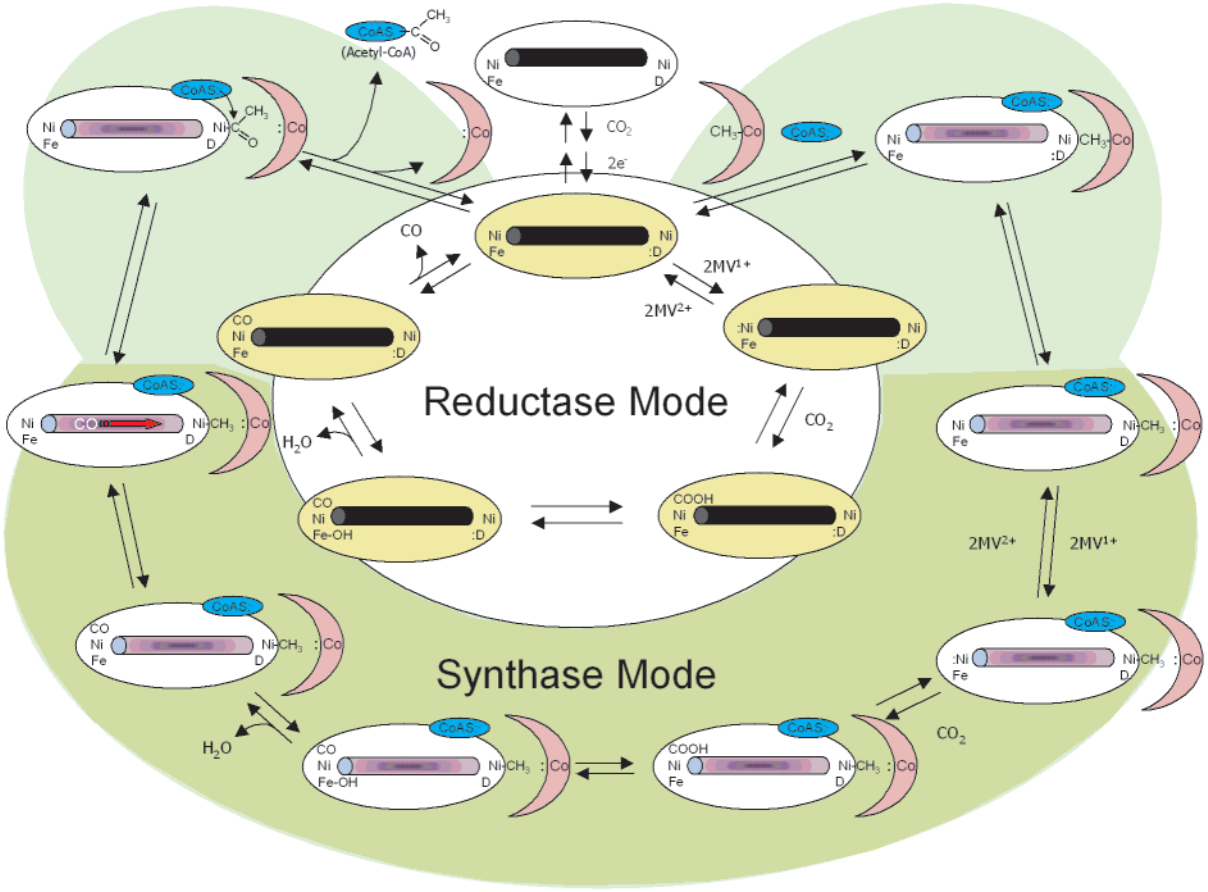

FIGURE 7: Unified ACS reductase/synthase catalytic cycle. ACS in the inactive, reductase, and synthase modes is colored gray, yellow, and lavender, respectively. The tunnel is black when the active sites are uncoupled, purple when they are coupled. The binding of CO_2 and subsequent reduction activates ACS. The reductase catalytic cycle is enclosed in the yellow oval and involves reduction, CO_2 binding, and release of CO (the order indicated is likely but not established). The synthase mechanism is shown on the green background, and involves: (i) the binding of synthase substrates; (ii) the methyl group transfer reaction; (iii) the C-cluster reductase steps (highlighted by a light-green background); (iv) CO migration through the tunnel to the A-cluster; (v) CO insertion into a Ni-methyl bond; vi) reductive elimination by CoA; and (vii) formation of the product (again, the indicated order is likely but not established).

and at ~ 1.7 times the native rate (Figure 6). This indicates that the burst reaction depends on the presence of the Ni of the A-cluster.[4]

In summary, our study reveals that a CO_2-dependent reduction event activates ACS for catalysis. In the absence of the synthase substrates CH_3−CP and CoA, active ACS is in reductase mode, where it reacts with $2MV^{1+}$ and CO_2 to produce and release CO. If the synthase substrates are present, they dock onto ACS, triggering conversion to synthase mode. Triggering reroutes CO through the tunnel to the A-cluster rather than releasing it into solution, alters the CO_2 kinetic parameters at the C-cluster, and activates an unidentified redox reaction that consumes MV^{1+}. These events are illustrated in Figure 7.

We were intrigued that the rate of CO production is synchronized with that of acetyl-CoA synthesis when ACS is A → C coupled. Are the two rates are fortuitously synchronized, or does the synthase reaction require synchronization of rates? Given that the rates of numerous mechanistic steps vary with substrate concentrations, fortuitous synchronization would occur only at a particular set of substrate concentrations. In contrast, we found that the rates are synchronized under all conditions examined. Thus, we favor the latter case, as implied by the mechanism of Figure 7. The only apparent way to render the synchronization obligatory is to require that the synthase mechanism occur by an ordered sequence of steps, beginning with the binding of synthase substrates. We propose that these substrates remain bound during catalysis and that this maintains ACS in the synthase mode (the homologous ACS subunits found in *Methanosarcina barkeri* are isolated as a stable complex with CP and MT (*26*)). Another issue requiring further investigation is whether ACS returns to reductase mode after each synthase cycle (essentially oscillating between modes with each catalytic cycle). The mechanism of Figure 6 implies this, but it is also possible that ACS in synthase mode decays back to reductase mode at a rate that is slow relative to the k_{cat} for acetyl-CoA synthesis. It appears a distinct possibility that ordered mechanisms are generally required to synchronize the coupled active sites of multifunctional tunnel-containing enzymes.

[4] Phen treatment appears to remove Ni ions only from A-clusters in functional $\alpha\beta$ dimers. Thus, the residual burst magnitude may arise from nonfunctional dimers.

[5] Phen−ACS had 440 ± 40 units·mg^{-1} CO oxidation activity, 0.03 units·mg^{-1} synthase activity, and 0.01 spins/$\alpha\beta$ NiFeC EPR signal. The respective values for the corresponding native sample were 410 ± 50 units·mg^{-1}, 1.5 units·mg^{-1}, and 0.35 spins/$\alpha\beta$.

REFERENCES

1. Pan, P., Woehl, E., and Dunn, M. F. (1997) *Trends Biochem. Sci. 22*, 22−27.

2. Holden, H. M., Thoden, J. B., and Raushel, F. M. (1999) *Cell. Mol. Life Sci. 56*, 507−522.
3. Krahn, J. M., Kim, J. H., Burns, M. R., Parry, R. J., Zalkin, H., and Smith, J. L. (1997) *Biochemistry*, *36*, 11061−11068.
4. Kappock, T. J., Ealick, S. E., and Stubbe, J. (2000) *Curr. Opin. Chem. Biol. 4*, 567−572.
5. Lindahl, P. A., and Chang, B. (2001) *Orig. Life Evol. B. 31*, 403−434.
6. Huber, C., and Wächtershäuser, G. (1997) *Science 276*, 245−247.
7. Wächtershäuser, G. (1988) *Microbiol. Rev. 52*, 452−484.
8. Ragsdale, S. W., and Kumar, M (1996) *Chem. Rev. 96*, 2515−2539.
9. Xia, J., Sinclair, J. F., Baldwin, T. O., and Lindahl, P. A. (1996) *Biochemistry 35*, 1965−1971.
10. Dobbek, H., Svetlitchnyi, V., Gremer, L., Huber, R., Meyer, O. (2001) *Science 293*, 1281−1285.
11. Lindahl, P. A., Ragsdale, S. W., and Münck, E. (1990) *J. Biol. Chem. 265*, 3880−3888.
12. Antonini, E., and Brunori, M. (1971) *Hemoglobin and Myoglobin in Their Reactions With Ligands*, North-Holland Publishing Co., Amsterdam.
13. Maynard, E. L., and Lindahl, P. A. (1999) *J. Am. Chem. Soc. 121*, 9221−9222.
14. Maynard, E. L., Sewell, C., and Lindahl, P. A. (2001) *J. Am. Chem. Soc. 123*, 4697−4703.
15. Lundie, L. L., Jr., and Drake, H. L. (1984) *J. Bacteriol. 159*, 700−703.
16. Morton, T. A., Runquist, J. A., Ragsdale, S. W., Shanmugasundaram, T., Wood, H. G., and Ljungdahl, L. G. (1991) *J. Biol. Chem. 266*, 23824−23828.
17. Lu, W. P., Schiau, I., Cunningham, J. R., and Ragsdale, S. W. (1993) *J. Biol. Chem. 268*, 5605−5614.
18. Roberts, D. L, Zhao, S. Y., Doukov, T., and Ragsdale, S. W. (1994) *J. Bacteriol. 176*, 6127−6130.
19. Blair, J. A., and Saunders, K. J. (1970) *Anal. Biochem. 34*, 376−381.
20. Gupta, V. S., and Huennekens, F. M. (1967) *Arch. Biochem. Biophys. 120*, 712−718.
21. Budavari, S. (1989) *The Merck Index*, 3rd ed., Merck & Co., Inc., Rahway, NJ.
22. Butler, J. N. (1982) *Carbon Dioxide Equilibria and Their Applications*, Addison-Wesley, Reading, MA.
23. Shin, W., and Lindahl, P. A. (1992) *J. Am. Chem. Soc. 114*, 9718−9719.
24. Barondeau, D. P., and Lindahl, P. A. (1997) *J. Am. Chem. Soc. 119*, 3959−3970.
25. Anderson, M. E., and Lindahl, P. A. (1994) *Biochemistry 33*, 8702−8711.
26. Grahame, D. A., Khangulov, S., and Demoll, E. (1996) *Biochemistry 35*, 593−600.

BI015604+